Double-diffusive lock-exchange gravity currents

Nathan Konopliv, Presenting Author and Eckart Meiburg

Department of Mechanical Engineering,
University of California Santa Barbara
meiburg@engineering.ucsb.edu

Abstract

The dynamics of double-diffusive gravity currents exhibiting the fingering instability were examined using 2D and 3D simulations of a lock exchange initial configuration. It was found that although the spreading of the currents was governed by a balance of buoyancy and turbulent drag forces, currents with more intense fingering spread faster than those with less intense or no fingering. This was due to an increase in the buoyancy of the currents with stronger fingering, which had a stronger effect than the increased drag. The fingering also affected the thickness of the currents, with more fingering corresponding to thinner currents. We found that in 3D, fluxes were higher than in 2D, so that currents with the same parameters exhibited the effects of stronger fingering in 3D.

1 Introduction

Recent decades have seen rapid growth in our understanding of the dynamics of single-component gravity currents (Benjamin, 1968; Linden, 2012), based on laboratory experiments (Huppert and Simpson, 1980), field observations (Huppert (2006) and references therein), high-resolution numerical simulations (Meiburg et al., 2015), and novel theoretical approaches (Borden and Meiburg, 2013). These investigations have elucidated the dynamical force balances governing the various stages of single-component gravity current flows, as well as their front velocity, mixing properties and energy budgets. By comparison, multicomponent gravity currents remain much less well understood, in spite of their importance in natural settings and engineering applications, such as river plumes, oceanic overflows and desalination plants. Most of the research on two-component gravity currents to date has focused on the influence of a particulate phase, and on the role of particle settling in triggering buoyancy reversal in such flows (Meiburg and Kneller, 2010). On the other hand, very few investigations have focused on the effects of double-diffusion on the dynamics of gravity currents driven by temperature and salinity differences.

Double-diffusion is known to give rise to a host of complex dynamical phenomena in nominally stably stratified thermohaline systems (Radko, 2013). At the most basic level, a fingering interface forms when the slowly diffusing component is unstably stratified, while a diffusive interface emerges for an unstable stratification of the faster diffusing component. The subsequent evolution of the convective flow can produce such interesting features as collective fingering instabilities, staircases and horizontal intrusions. To date, double-diffusive convection has primarily been explored for base states in which the fluid is at rest. On the other hand, for base states in the form of gravity currents, characterized by sharp fronts, pronounced temperature and salinity gradients, as well as strong shear, we might expect the evolution of double-diffusive convection to proceed quite differently. This was confirmed in the laboratory experiments of double diffusive gravity currents by Maxworthy (1983), who explored the scaling laws and force balances governing both fixed volume and constant flow rate double-diffusive currents and intrusions.

Here we summarize some of the key findings, while a more detailed discussion of double-diffusive gravity currents is presented in Konopliv and Meiburg (2016).

2 Problem Setup

We perform direct numerical simulations of full-depth, double-diffusive lock exchange gravity currents, as sketched in figure 1. The left half of the domain initially contains the lighter, hot and salty fluid of density ρ_1, whereas the heavier, cold and fresh fluid of density ρ_2 is located on the right. We always refer to the faster diffusing component as "heat" and the slower diffusing component as "salt." In dimensionless units, the domain extends from $x = -30$ to $x = 30$, and it has a height of one. When the lock is released, the lighter fluid forms a buoyant current that propagates towards the right along the top wall, whereas the denser fluid propagates towards the left along the bottom wall.

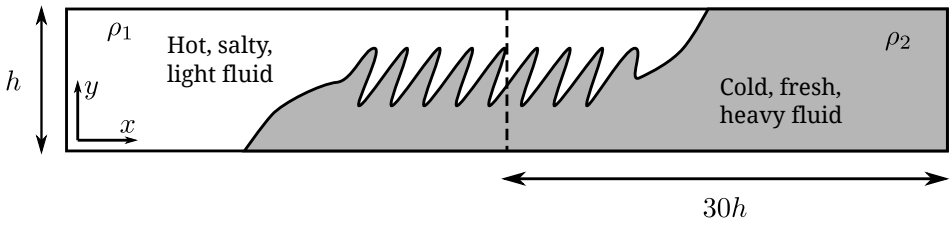

Figure 1: Sketch of the lock exchange flow under consideration. The left reservoir is initially filled with light, hot and salty fluid, while the right reservoir contains dense, cold and fresh fluid. Upon removal of the gate (represented by the dashed line), the hot and salty fluid forms a right-moving buoyant current along the top wall, while the cold and fresh fluid propagates to the left along the bottom wall. The interface separating the two currents may be subject to double-diffusive fingering.

We employ the Navier-Stokes equations in the Boussinesq approximation, along with convection-diffusion equations for heat and salinity. In order to nondimensionalize these equations, we use the height of the domain h and the buoyancy velocity $U_b = \sqrt{g'h}$, where $g' = g(\rho_2 - \rho_1)/\rho_0$ and $\rho_0 = (\rho_1 + \rho_2)/2$. The governing dimensionless parameters

$$Re \equiv \frac{U_b h}{\nu} \quad , \quad Pe_T \equiv \frac{U_b h}{k_T} \quad , \quad Pe_S \equiv \frac{U_b h}{k_S} \quad , \quad \tau \equiv \frac{k_S}{k_T} \equiv \frac{Pe_T}{Pe_S} \tag{1}$$

have the form of a Reynolds and two Peclet numbers. Additionally, it is convenient to define the diffusivity ratio τ. Here ν denotes the kinematic viscosity of the fluid, while k_T and k_S represent the diffusivities of heat and of salt, respectively. An additional parameter,

$$R_{\rho 0} = \frac{\alpha \Delta T}{\beta \Delta S} \ , \tag{2}$$

arises through the initial condition and represents the ratio of the density loadings due to temperature and salinity.

3 Results

We define the length $L(t)$ of the rightward propagating buoyant top current as the distance from the gate to the current tip, which is taken as the most advanced location with a dimensionless temperature of at least 0.05. For a constant initial stability ratio $R_{\rho 0} = 1.07$, figure 2a displays the ensemble-averaged current length $L(t)$ as function of τ. Keeping in

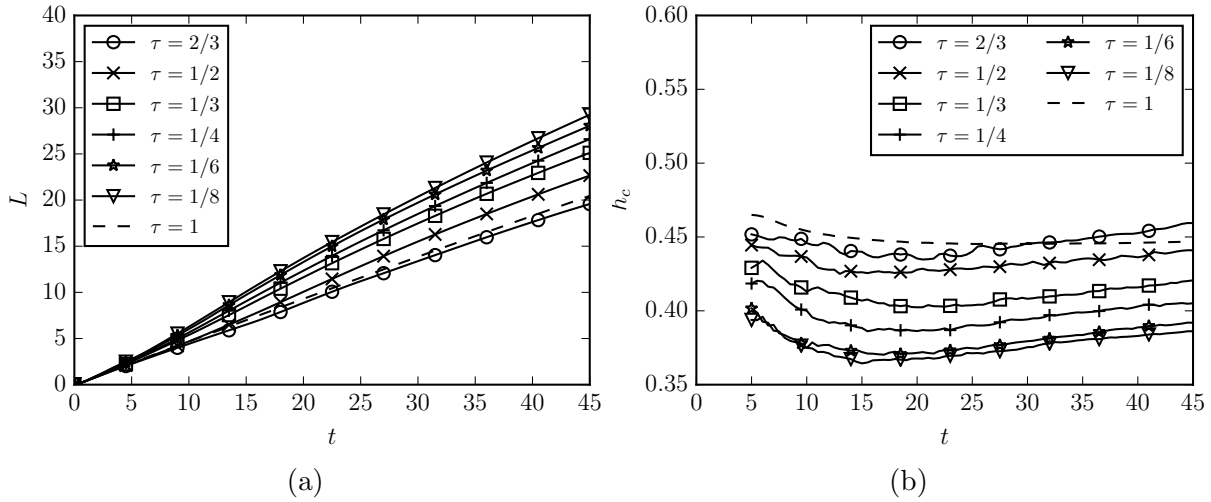

Figure 2: Current length *vs.* time (a), and current thickness *vs.* time (b) for $R_{\rho 0} = 1.07$ with varying τ. Smaller values of τ, i.e., more strongly double-diffusive currents, result in larger front velocities and thinner currents. The single-diffusive case corresponds to $\tau = 1$.

mind that $\tau = 1$ corresponds to classical, single-diffusive gravity currents, we find that strongly double-diffusive currents propagate up to 50% faster than classical currents. We expect double-diffusion to affect the current velocity via two opposing mechanisms: On one hand, double-diffusion can increase the density contrast between a current and its ambient environment, which in turn will increase the current velocity. This is due to the release of potential energy stored in the salinity field, which drives the fingering. At the same time, double-diffusive fingering will increase the turbulent drag acting on the current, which should have a retarding effect. Interestingly, figure 2a indicates that the current velocity does not vary monotonically with τ. For τ-values slightly less than one, i.e. for weakly double-diffusive currents, we observe the current length to grow more slowly than for single-diffusive currents, whereas for strongly double-diffusive currents it grows more rapidly. This suggests that τ affects the balance between buoyancy and turbulent drag in a nonlinear fashion.

In order to provide quantitative evidence for the scenario outlined above, we now discuss the effective density profile of the current. Towards this end, figure 3a displays vertical ρ-profiles averaged in the streamwise direction from the gate position to the location half a channel height behind the current front. This figure indicates that the dimensionless density of the strongly double-diffusive ($\tau = 1/8$) top current can reach values as low as -1.5 near the upper boundary, far below the left reservoir value of $\rho = 0$. Similarly, the current density near the lower wall significantly exceeds the value $\rho = 1$ in the right reservoir. The weakly double-diffusive ($\tau = 2/3$) current, on the other hand, loses heat and salinity at approximately the same rate, so that its effective density varies from $\rho = 1$ near the bottom wall to $\rho = 0$ near the top wall, similar to the single-diffusive gravity current. This increased buoyancy for the strongly double-diffusive current is consistent with the results shown in figure 2a, where the strongly double-diffusive gravity current was seen to propagate much faster than its weakly double-diffusive counterpart. However, to fully understand the behavior shown in figure 2a, we will also have to consider the potentially higher drag acting on the strongly double-diffusive current, as a result of the fingering. We will return to this point further below.

In a top current with strong double-diffusive fingering, fingers transport salt out of the top current and into the ambient below. This transport of salt results in the formation

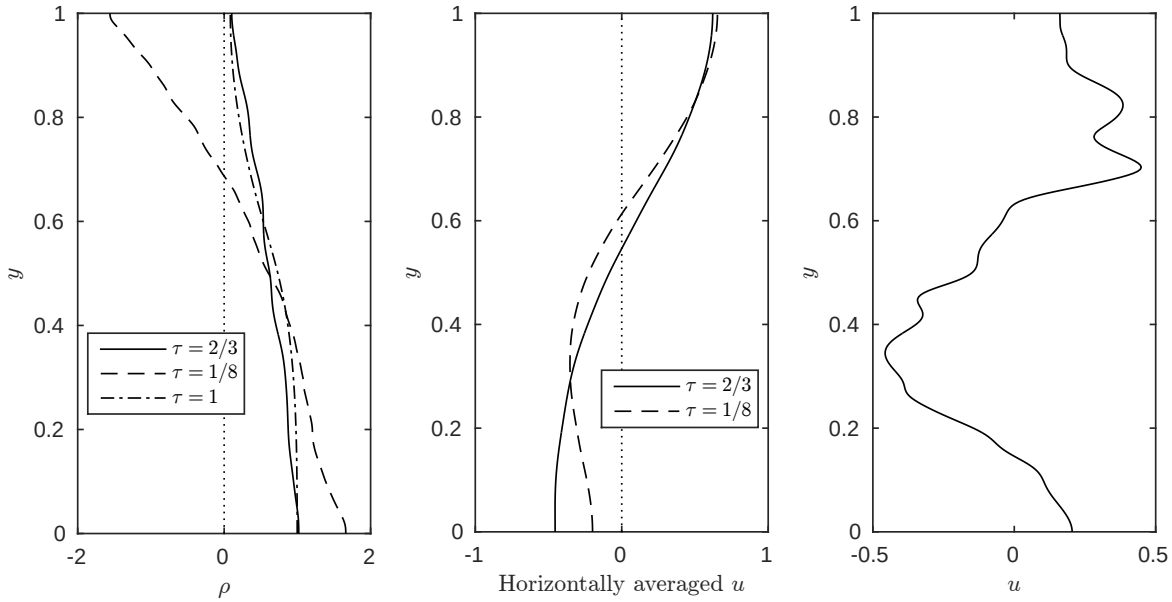

(a) (b) (c)

Figure 3: Horizontally averaged ρ-profiles (a), and horizontally averaged u-profiles (b), for simulations with $R_{\rho 0} = 1.07$ and $\tau = 2/3$, $1/8$ at $t = 45$. In each frame, the more strongly double-diffusive current develops a pronounced three-layer structure. Frame (c) shows the u-profile at $x = 3$ for a simulation with $R_{\rho 0} = 1.07$ and $\tau = 1/8$. The right-moving, very dense current next to the bottom wall is clearly visible, while the left-moving current containing fluid from the right reservoir has been deflected upwards, and away from the wall.

of a dense pool near the bottom of the gate region. The formation of this pool of high-density fluid along the bottom wall, which is responsible for the large densities seen in figure 3a and can also be observed in figure 4, strongly modifies the structure of the flow field. Since this fluid is significantly denser than the fluid in the right reservoir, it tends to spread horizontally along the bottom wall in both directions, and *below* the fluid of the right reservoir. Consequently, it deflects the left-moving current of right reservoir fluid upwards and away from the bottom wall. In this fashion, the flow field to the right of the original gate location acquires an effective three-layer structure, with a right-moving, light current along the top wall made up of warm and increasingly less salty fluid, a left-moving intermediate density current in the center of the channel, and a pool of very dense, cold and salty fluid spreading horizontally along the bottom wall.

This emerging three-layer structure for strongly double-diffusive gravity currents ($\tau = 1/8$) is confirmed by the horizontally averaged u-velocity profiles shown in figure 3b. The weakly double-diffusive gravity current ($\tau = 2/3$), on the other hand, exhibits a clear two-layer structure, with a light top current moving to the right, and a dense bottom current moving to the left. The right-moving, dense current along the bottom wall can be clearly recognized in the local velocity profile of figure 3c for the strongly double-diffusive current.

The thickness of the buoyant top current can be defined by a horizontal average of the location of the current interface, where the current interface is defined as the y-location above which the horizontal volume flux in the positive x-direction reaches a maximum. The condition of zero net horizontal volume flux implies that this y-location also maximizes the horizontal volume flux in the negative x-direction below. For a representative current with $R_{\rho 0} = 1.07$ and $\tau = 1/4$, figure 4 shows that the y-position of the interface

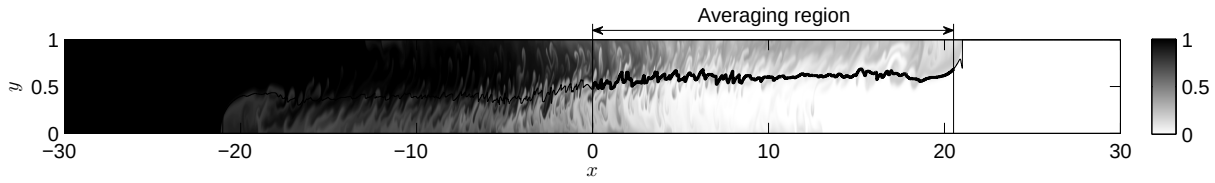

Figure 4: Salinity concentration for a current with $R_{\rho 0} = 1.07$ and $\tau = 1/4$, at $t = 35$. The current interface, evaluated as described in the text, is drawn as a solid line. To obtain effective current properties such as temperature, salinity and thickness, we average from the gate location to half a channel height behind the current tip.

remains nearly constant over the length of the current. In order to eliminate artifacts due to the current front, we take this streamwise average from the gate location to the position half a channel height behind the current front. We furthermore remark that, due to the initial transient flow evolution, a meaningful current thickness can be identified only after $t \approx 5$.

Figure 2b displays the current thickness as a function of time for $R_{\rho 0} = 1.07$ and various values of τ. During the acceleration phase until $t \approx 15 - 20$, the current thickness decreases slightly, whereas subsequently it shows a mild increase as the current decelerates. While weakly double-diffusive currents have a thickness similar to that of single-diffusive currents, more strongly double-diffusive currents are seen to be increasingly thinner, as a result of the transition from a two-layer to a three-layer structure of the flow field, as described below.

Following the approach of Maxworthy (1983), the turbulent drag due to vertical transport of horizontal momentum as a result of double-diffusive fingering can be estimated in dimensional terms as

$$F_{dd} \sim \rho_0 U V L \sim \rho V L \frac{\mathrm{d}L}{\mathrm{d}t} \ , \tag{3}$$

where U represents the horizontal velocity scale. The buoyancy force can be estimated by integrating the hydrostatic pressure difference between an idealized current shape and the ambient, as shown by Maxworthy (1983)

$$F_b \sim \Delta \rho g h_c^2 \ . \tag{4}$$

We obtain the spreading relationship for a current governed by a fingering drag-buoyancy balance by combining (3) and (4)

$$\rho V L \frac{\mathrm{d}L}{\mathrm{d}t} \sim \Delta \rho g h_c^2 \ . \tag{5}$$

Nondimensionalizing and integrating gives

$$\widetilde{L}^2 - \widetilde{L}_s^2 \sim \int_{\widetilde{t}_s}^{\widetilde{t}} \frac{\gamma(\widetilde{t}')}{\widetilde{V}} \mathrm{d}\widetilde{t}' \ , \tag{6}$$

where $\widetilde{t}_s$ indicates the transition time beyond which (6) first becomes valid, and $\widetilde{L}_s$ represents the corresponding transition length. This balance corresponds to the one proposed by Maxworthy (1983), except that here we assume h_c to be constant, as discussed in the previous section, and we employ $U \sim \mathrm{d}L/\mathrm{d}t$ instead of $U \sim L/t$.

In order to test for this turbulent drag-buoyancy balance, we carried out a long simulation until $t = 190$ in a large control volume $x \in [-60, 60]$, for parameter values $R_{\rho 0} = 1.50$

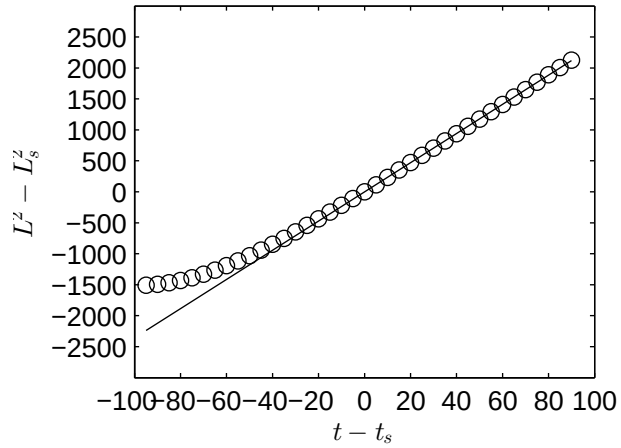

Figure 5: Test for a turbulent drag-buoyancy balance at later times. In the figure, $t_s = 100$ and L_s is the length of the current at $t = t_s$. The fact that the data forms a straight line through the origin shows that (6) holds in this time range.

and $\tau = 1/8$, which result in a moderate amount of fingering. Figure 5 plots the two sides of (6) against each other, with the additional assumption that γ/V does not depend on time, which holds approximately for this simulation. In order to provide sufficient time for the transition to the turbulent drag-buoyancy balance to be completed, we choose $t_s = 100$, with $\tilde{L}_s$ denoting the current length at $t = t_s$. The agreement of the simulation data with the straight line through the origin in figure 5 confirms the turbulent drag-buoyancy balance for long times.

All of the simulations discussed up to this point were two-dimensional in nature. In order to explore the qualitative and quantitative agreement between two- and three-dimensional flows, we conducted a single three-dimensional run for $R_{\rho 0} = 1.07$ and $\tau = 1/8$ in a smaller domain. A visualization of the salinity isosurfaces at $t = 14$ is shown in figure 6. The 3D current exhibited similar characteristics to a 2D current with stronger fingering than it would have had for the same parameters. This was confirmed by examining such quantities as current thickness, temperature and salinity and using spanwise-averaged results to compare with 2D. Our finding that the three-dimensional current is similar to its two-dimensional counterpart but exhibits stronger fingering is consistent with results presented in Radko et al. (2015) for flows with stochastic shear. This author's work shows that fingering fluxes are larger in unsheared three-dimensional flows as compared to two dimensions, but that fluxes in a sheared three-dimensional environment are similar to two-dimensional fluxes in an unsheared environment. This is mainly due to the fact that shear causes three-dimensional fingers to align into salt sheets in the plane of the shear Linden (1974), since modes with nonzero wavenumber in this direction are damped. As a result, shear effectively reduces the dimensionality of the fingering from three to two dimensions, thereby reducing the flux by a factor of 2 to 3 (Radko et al. (2015)). In two-dimensional gravity currents, the lack of the third dimension prevents any sheets from forming, and only modes with nonzero wavenumbers in the streamwise direction can grow. However, these modes will be damped in comparison to three dimensions, so that fluxes will be lower in the sheared two-dimensional environment. This implies that our work may have more places to be potentially applicable, since the governing parameters in nature may not be as favorable to strong fingering as they were in our simulations, but the presence of a third dimension will enhance double-diffusive fluxes.

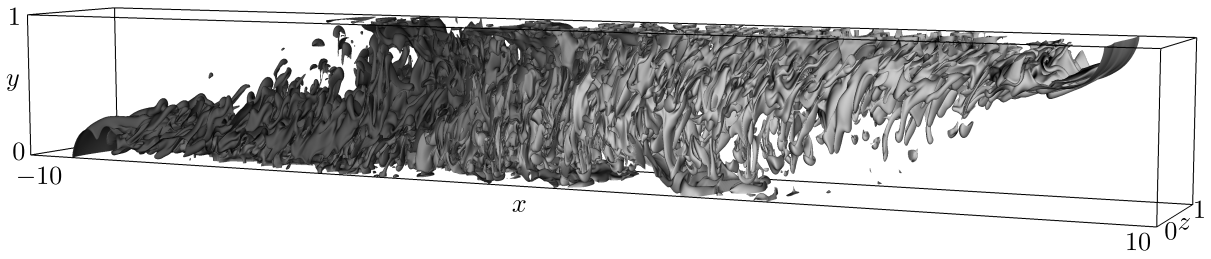

Figure 6: Three-dimensional isosurfaces of the salinity concentration for a 3D double-diffusive current. From dark to light, the contour values are 0.1, 0.3, 0.5, 0.7 and 0.9.

References

Benjamin, T. (1968). Gravity currents and related phenomena. *J. Fluid Mech.*, 31:209–248.

Borden, Z. and Meiburg, E. (2013). Circulation based models for boussinesq gravity currents. *Phys. of Fluids*, 25(10).

Huppert, H. (2006). Gravity currents: a personal perspective. *J. Fluid Mech.*, 554:299–322.

Huppert, H. and Simpson, J. (1980). The slumping of gravity currents. *J. Fluid Mech.*, 99:785–799.

Konopliv, N. and Meiburg, E. (2016). Double-diffusive lock-exchange gravity currents. *J. Fluid Mech.*, 797:729–764.

Linden, P. (1974). Salt fingers in a steady shear flow. *Geo. & Astro. Fluid Dyn.*, 6(1):1–27.

Linden, P. (2012). Gravity currents – theory and laboratory experiments. In Chassignet, E., Cenedese, C., and Verron, J., editors, *Buoyancy-Driven Flows*, pages 13–51. Cambridge University Press.

Maxworthy, T. (1983). The dynamics of double-diffusive gravity currents. *J. Fluid Mech.*, 128:259–282.

Meiburg, E. and Kneller, B. (2010). Turbidity currents and their deposits. *Ann. Rev. Fluid Mech.*, 42:135–156.

Meiburg, E., Radhakrishnan, S., and Nasr-Azadani, M. (2015). Modeling gravity and turbidity currents: Computational approaches and challenges. *App. Mech. Rev.*, 67(4):040802.

Radko, T. (2013). *Double-Diffusive Convection*. Cambridge University Press.

Radko, T., Ball, J., Colosi, J., and Flanagan, J. (2015). Double-diffusive convection in a stochastic shear. *J. Phys. Oceanogr.*, 45(12):3155–3167.